Optimizing the Reinforcement of Polymer-Based Nanocomposites by Graphene

Lei Gong,[†] Robert J. Young,[†,*] Ian A. Kinloch,[†] Ibtsam Riaz,[‡] Rashid Jalil,[‡] and Kostya S. Novoselov[‡]

[†]Materials Science Centre, School of Materials and [‡]School of Physics and Astronomy, University of Manchester, Oxford Road, Manchester M13 9PL, U.K.

ABSTRACT The stress transfer between the internal layers of multilayer graphene within polymer-based nanocomposites has been investigated from the stress-induced shifts of the 2D Raman band. This has been undertaken through the study of the deformation of an ideal composite system where the graphene flakes were placed upon the surface of a polymer beam and then coated with an epoxy polymer. It is found that the rate of band shift per unit strain for a monolayer graphene flake is virtually independent of whether it has one or two polymer interfaces (*i.e.*, with or without an epoxy top coating). In contrast, the rate of band shift is lower for an uncoated bilayer specimen than a coated one, indicating relatively poor stress transfer between the graphene layers. Mapping of the strain in the coated bilayer regions has shown that there is strain continuity between adjacent monolayer and bilayer regions, indicating that they give rise to similar levels of reinforcement. Strain-induced Raman band shifts have also been evaluated for separate flakes of graphene with different numbers of layers, and it is found that the band shift rate tends to decrease with an increase in the number of layers, indicating poor stress transfer between the inner graphene layers. This behavior has been modeled in terms of the efficiency of stress transfer between the inner graphene layers. Taking into account the packing geometry of polymer-based graphene nanocomposites and the need to accommodate the polymer coils, these findings enable the optimum number of graphene layers for the best reinforcement to be determined. It is demonstrated that, in general, multilayer graphene will give rise to higher levels of reinforcement than monolayer material, with the optimum number of layers depending upon the separation of the graphene flakes in the nanocomposite.

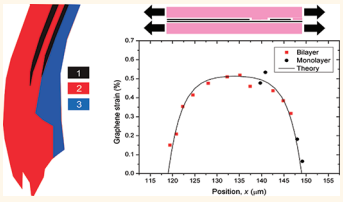

KEYWORDS: graphene · Raman spectroscopy · deformation · nanocomposites · micromechanics

Graphene is one of the most exciting topics in materials science and condensed matter physics[1] with good prospects for applications.[2,3] It was first isolated in Manchester in 2004,[4] and since that time the majority of the research effort has been concentrated upon investigating its electronic properties, aimed at using graphene in applications such as electronic devices.[5,6] In recent times, however, because of its interesting and unusual electronic properties, bilayer graphene has attracted particular interest.[7,8]

The mechanical properties of graphene are also very promising, with AFM nanoindentation of graphene layers finding a Young's modulus on the order of 1 TPa and an intrinsic strength of around 130 GPa.[9] These properties make it one of the stiffest and strongest materials ever measured and an ideal candidate for use as a reinforcement in high-performance composites. It is now established that Raman spectroscopy is one of the best methods of both characterizing graphene and following its subsequent deformation. Relatively strong, well-defined resonance Raman spectra are obtained even from single atomic graphene layers, and the technique can be used to differentiate between monolayer, bilayer, trilayer, and many-layer material, from the shape and position of the 2D (or G′) Raman band.[10,11] It is also found that the positions of the Raman bands in graphene shift with stress[12−25] and that stress-induced Raman band shifts can consequently be employed to determine the stress in the material and so estimate its effective Young's modulus.[24]

Stress-induced Raman band shifts have been employed widely to follow the deformation of fibers such as high-modulus polymer[26,27] and carbon fibers[28,29] in polymer matrix composites. It is possible to explore the fundamental micromechanics of fiber reinforcement and a wide range of phenomena including fiber fragmentation,[30] breakdown of the fiber−matrix interface,[31,32] fiber−fiber interactions,[33] and fiber−crack interactions. This approach has more recently been extended to evaluate the reinforcement of polymers by carbon nanotubes for which large stress-induced band shifts are also found.[34,35]

In recent papers[36,37] we have demonstrated unambiguously that stress transfer takes place from the polymer matrix to monolayer graphene, showing that the

* Address correspondence to robert.young@manchester.ac.uk.

Received for review October 11, 2011 and accepted February 26, 2012.

Published online February 26, 2012
10.1021/nn203917d

graphene has the capability of acting as a reinforcing phase in nanocomposites. This previous work has been undertaken through the use of model polymer nanocomposites in which monolayers of graphene were prepared by exfoliation and placed on a polymer beam with a thin layer of polymer spin-coated on the top to make a sandwich structure. Stress transfer from the polymer matrix to the graphene was monitored from the shift of the 2D Raman band. It was demonstrated, by following the variation of strain in the graphene across a flake, that at low strains continuum mechanics could be applied to this nanocomposite system,[36] and the behavior could be modeled using a simple shear-lag approach.[38] At higher levels of strain, failure of the graphene/polymer interface appeared to occur.[36] Since the size of the Raman laser spot employed was only on the order of 1 μm compared to flake dimensions in excess of 100 μm^2, it was also possible to map the strain distribution over a relatively large flake during deformation.[37] It was found that at relatively low strains ($\leq$0.4%) the strain distribution in the flake was relatively uniform, with the strain in the flake being the same as the strain in the matrix. At higher strains, however, the strain distribution became nonuniform due probably to fragmentation of the polymer matrix.[37] Our research on Raman band shifts in these model graphene nanocomposites has therefore demonstrated clearly that individual exfoliated flakes of graphene have the capability of reinforcing a polymer matrix. It appears that the approach can also be extended to higher loadings of graphene from other sources since there are recent reports of significant shifts of the Raman G band being obtained during the deformation of a nanocomposite consisting of ~0.1% of graphene platelets, obtained by the thermal reduction of graphene oxide, in a poly(dimethylsiloxane) matrix[39] and upon the deformation of graphene oxide paper infiltrated with glutaraldehyde.[40]

As stress transfer to monolayer graphene is now relatively well understood, the aim of this present study was to evaluate and compare the levels of reinforcement in nanocomposites by exfoliated graphene flakes consisting of a different numbers of layers, paying particular attention to the behavior of bilayer, trilayer, and many-layer graphene materials. In one of the first investigations of the deformation of exfoliated graphene flakes, Ni *et al.*[12] found that the shift rate of trilayer graphene upon a polyester film was less than that of the monolayer material. Tsoukleri and co-workers[16] followed the deformation of polymer-coated graphene flakes on a PMMA beam and found that the shift rate of the 2D band for many-layer material (that they termed "graphite") was lower than that for monolayer graphene. Moreover, they found that the band shift rate for the many-layer graphene without a top coat (*i.e.*, a polymer interface on only one surface of the flake) was very low. Procter *et al.*[17] followed the shifts of the G and 2D bands of graphene, with different numbers of layers, supported uncoated on the surface of 100 μm thick silicon wafers subjected to hydrostatic pressure. The graphene followed the biaxial compression of the surface of the silicon wafer during the pressurization since the thickness of the graphene was very much less than that of the silicon. Procter *et al.*[17] found that the highest rate of band shift (per unit pressure) was for a graphene monolayer. This band shift rate for bilayer graphene on the silicon substrate was slightly lower than that of the monolayer, whereas the shift rate of their "few-layer" graphene was only half that of the monolayer material. It was suggested[17] that this lower rate for few-layer material might be due to poor adhesion with the substrate. It is clear, therefore, that there is a need for a systematic study on the effect of the number of layers in graphene upon its deformation behavior and hence the ability to reinforce polymer matrices with graphene.

RESULTS AND DISCUSSION

Deformation of the graphene was undertaken by bending polymer beams on which flakes had been deposited. This leads to an axial strain in the graphene, whereas the stress is somewhat biaxial in nature due to Poisson's contraction effects. The crystallographic orientation of the flakes was not taken into account. Since all measurements were undertaken under similar conditions, all data are quoted in terms of graphene strain and only the relative band shifts during deformation were considered.

The shift of the 2D band with tensile strain for different monolayer and bilayer graphene flakes, deformed both before and after applying the SU-8 top coat, is shown in Figure 1. The maximum strain in this case was 0.4%, which is known to be below the level of strain at which debonding of the flakes or matrix polymer cracking can occur.[37] It can be seen from Figure 1a that the shift of the 2D Raman band for the graphene monolayer is -59 cm^{-1}/% strain and similar with and without the polymer top coat. It is well established that the rate of shift per unit strain of the 2D Raman band for monolayer graphene depending upon the crystallographic orientation of the monolayer relative to the strain axis[20−22] and this value is within the range found by others, in both uncoated and coated specimens. In contrast, it is shown in Figure 1b that when the 2D Raman band is fitted to a single peak, the rate of shift per unit strain for an uncoated graphene bilayer (-31 cm^{-1}/% strain) is significantly less that of the same flake deformed after being coated (-53 cm^{-1}/% strain). The implications of this observation for the bilayer is that stress transfer between the polymer substrate and the graphene is relatively good, as has been found before,[36] but that the efficiency of stress transfer between the lower and upper graphene layers is relatively poor. This is

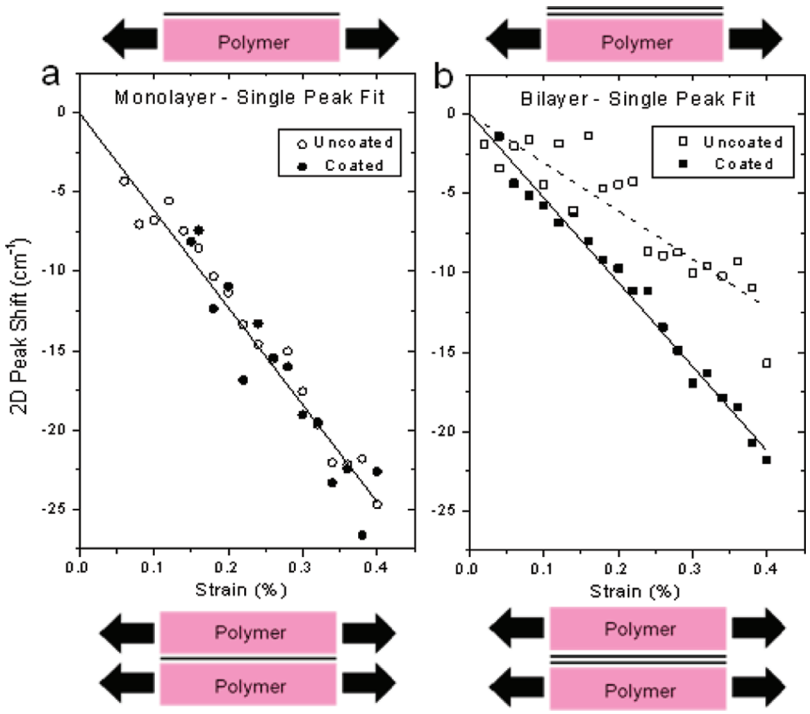

Figure 1. Shift with strain of the 2D Raman band of the graphene fitted to a single peak during deformation upon the PMMA beam (laser excitation 633 nm). (a) A graphene monolayer deformed before and after coating with SU-8. (b) A graphene bilayer deformed before and after coating with SU-8. (Schematic diagrams of the deformation of the uncoated (above) and coated (below) graphene are also included).

not an issue for the monolayer in Figure 1a, where the presence of the top coat makes no difference to the band shift rate.

The band shift data in Figure 1b are for the 2D band for the bilayer graphene fitted to a single peak. It is well established[10,11] that the 2D band for the bilayer material can be fitted to four peaks, as shown in the Supporting Information. Details of this band are also shown in the Supporting Information before and after deformation for the specimen both uncoated and coated. It is found that the four peaks making up the band shift during deformation but remain otherwise unchanged (except for small relative intensity changes), demonstrating that the A−B Bernal stacking is maintained during the deformation of the specimen, in both the uncoated and coated states. Similar behavior has been reported by Frank *et al.*,[25] although they did find evidence of local Bernal to non-Bernal transitions due possibly to cohesive failure of the multilayer graphene.

In order to gain further insight into the behavior of flakes with different numbers of graphene layers, the deformation of a single coated flake containing distinct regions of monolayer, bilayer, and trilayer graphene (identified before deformation) was first investigated. An optical micrograph of the flake is given in Figure 2a along with a schematic diagram in Figure 2b showing the different regions in the micrograph determined from both thickness contrast and Raman spectra. The 2D Raman spectra obtained from the monolayer, bilayer, and trilayer regions are shown in Figure 2c−e, respectively. It can be seen that the monolayer 2D band comprises a single peak, whereas the bilayer and trilayer 2D bands can be fitted to four[10,11] and six[11] sub-bands, respectively. In addition, a 2D band of a coated many-layer graphene flake (micrograph not shown) is given for reference in Figure 2f. The band in this case is similar to that of graphite.[11]

Figure 3 shows how the deformation of the middle of adjacent monolayer, bilayer, and trilayer regions of the flake in Figure 2 up to 0.4% strain was followed from the shifts of their 2D Raman bands. The advantage of doing this on the same flake is that it can be ensured that the orientation of the graphene is identical in each region (A−B Bernal stacking is confirmed from the forms of the 2D bands[11] in Figure 2c−f). The shift with strain of the four components of the bilayer graphene 2D band is shown in Figure 3a. The shift of the adjacent monolayer region is shown for comparison. The 2D1B and 2D2B sub-bands (labeled) are relatively weak and therefore are somewhat scattered, but it can be seen that the slopes of the two strong components 2D1A and 2D2A are similar to each other (−53 and −55 cm^{-1}/% strain, respectively) and also similar to the slope of the adjacent monolayer region (−52 cm^{-1}/% strain).

The 2D band shifts with strain of the four different coated graphene structures are given in Figure 3b, with the 2D band force fitted to a single Lorentzian peak in each, for comparison purposes. The many-layer graphene

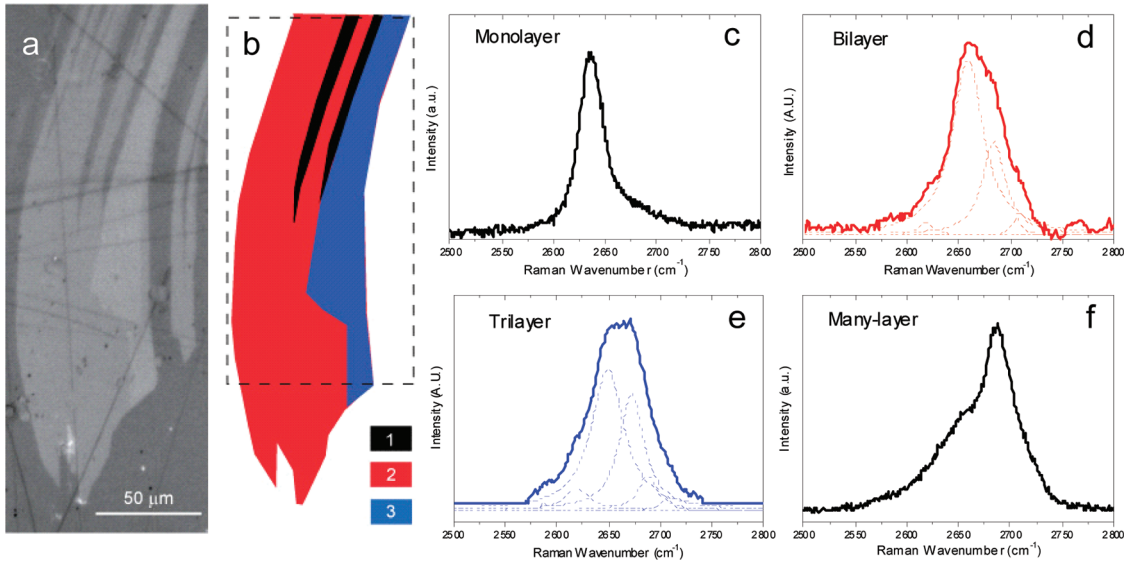

Figure 2. Graphene flake on a PMMA beam showing monolayer, bilayer, and trilayer regions. (a) Optical micrograph (the fine straight lines are scratches on the surface of the beam). (b) Schematic diagram of the flake highlighting the different areas (the rectangle shows the area of the flake over which the strain was mapped). (c–f) Raman spectra of the 2D band part of the spectrum for the monolayer, bilayer (fitted to 4 peaks), and trilayer regions (fitted to 6 peaks) and a multilayer graphene flake, elsewhere on the beam (laser excitation 633 nm).

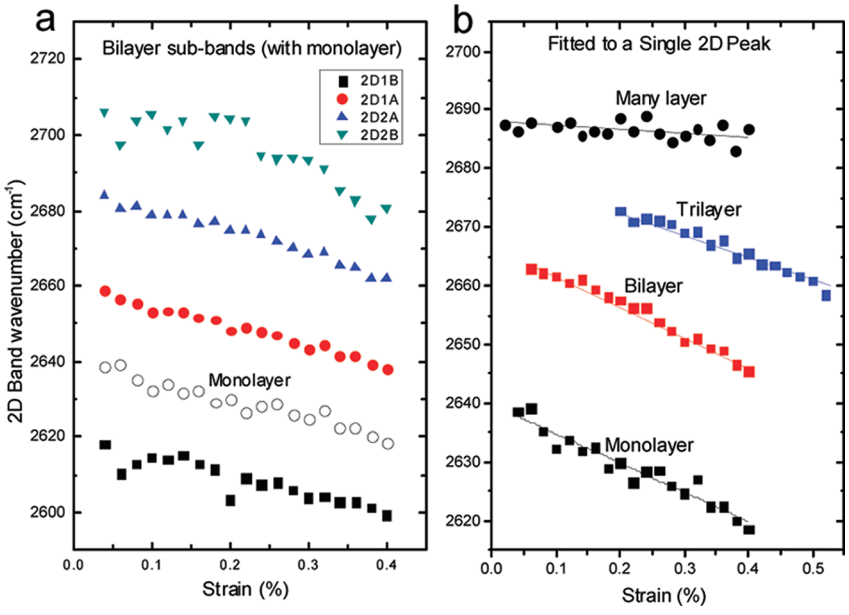

Figure 3. (a) Shift with strain of the four components of the 2D Raman band of the bilayer graphene shown on the specimen in Figure 2 along with the shift of the 2D band in an adjacent monolayer region on the same flake (laser excitation 633 nm). (b) Shifts with strain of the 2D band for adjacent monolayer, bilayer, and trilayers regions on the specimen in Figure 2, along with the shift with strain for the 2D band of a multilayer flake on the same specimen (all 2D bands were force fitted to a single Lorentzian peak).

was from a different region of the specimen, and the strain in the trilayer was offset since it was deformed after preloading of the beam to examine the behavior of other regions and so a permanent set had developed. The 2D Raman band positions at a given strain are offset from each other due to differences in the band structure of the different forms of graphene, as has been shown elsewhere.[10,11] It can also be seen that the slopes of the plots are similar for the monolayer and bilayer material (−52 and −53 cm^{-1}/% strain, respectively) but somewhat lower for the trilayer at −44 cm^{-1}/% strain. In contrast, the slope for the many-layer graphene is significantly lower, at around −8 cm^{-1}/% strain.

Although the data shown in Figures 1 and 3 suggest that the 2D band shift rates vary with the number of layers in the graphene and the presence or absence of a polymer top coat, there is always the possibility that such variations may be due to inhomogeneities or

uneven stress transfer due to slippage.[25] Variations in the band shift behavior are also known to occur due to differences in excitation wavelength, relative orientation of the graphene lattice to the straining direction, and direction of laser polarization.[14,15,21,22] Because of this, a systematic study was undertaken of the band shifts during deformation for more than 30 different graphene flakes on polymer beams in different orientations, consisting of different numbers of layers, both uncoated and with a polymer top coat. A different laser excitation was also employed (785 nm rather than 633 nm), and the data were carefully screened for evidence of slippage. Details of this investigation are given in the Supporting Information, and the relative 2D band shift rates with strain are summarized in Table 1.

For the uncoated specimens in Table 1, it can be seen that there is a decrease in the band shift rate for the flakes as the number of layers is increased from one to three. The shift rate data are more scattered for the multilayer flakes, as it is impossible to know the exact number of layers in such flakes. The shift rate for a graphite flake on the same uncoated specimen is also very low. In contrast the band shift rates are generally higher in the case of the coated specimen. The monolayer and bilayer flakes in the coated specimen have the same band shift rate within the limits of experimental error, and the band shift rate then decreases for the three-layer and multilayer flakes (again more scattered for the same reason as before). The shift rate for a graphite flake is again very low. The band shift behavior shown in Figures 1 and 3 is completely consistent with the comprehensive set of data in Table 1. Similarly Procter *et al.*[17] found that the band shift rate for (uncoated) bilayer graphene on the silicon substrate under pressure was slightly lower than that of the monolayer, whereas the shift rate of their "few-layer" graphene was only half that of the monolayer material. Although they suggested that that this lower rate for few-layer material could be due to poor adhesion with the substrate, the findings in Table 1 imply that it is more likely that this lower band shift rate is an inherent property of the few-layer material.

It is well established that, to a first approximation, the band shift rates in Table 1 can be related to the efficiency of stress transfer to the graphene.[24,36,39] All the data were obtained from the middle of the flakes and by eliminating any data showing slippage at the graphene–polymer interface. Differences with respect to the monolayer will therefore principally be a result of the efficiency of stress transfer between the different graphene layers (the effect of different crystallographic orientations of the graphene will lead to only minor differences).[14,21] This phenomenon is completely analogous to the efficiency of stress transfer between the different walls in multiwalled carbon nanotubes (MWNTs) analyzed by Zalamea, Kim, and Pipes.[41] They introduced a parameter k_i that characterizes the efficiency of stress transfer; for perfect transfer between the walls, $k_i = 1$ and for no stress transfer, $k_i = 0$. This analysis has been used to successfully model[42] stress transfer between the outer and inner walls of double-walled carbon nanotubes (DWNTs), made by the pea-pod route,[43] in a nanocomposite. It is shown in the Supporting Information that it is relatively easy to adapt this theory to model stress transfer between the layers of multilayer graphene.

TABLE 1. Measured 2D Raman Band Shift Rates (with standard deviations) for the Uncoated and Coated Graphene Nanocomposite Specimens Described in the Supporting Information (laser excitation 785 nm)[a]

no. of layers	coating	$d\omega_{2D}/d\varepsilon$ (cm^{-1}/% strain)	no. of flakes studied
1	uncoated	-48.8 ± 2.5	3
2	uncoated	-38.9 ± 2.4	3
3	uncoated	-32.4 ± 0.4	2
many	uncoated	-37.4 ± 8.2	3
graphite	uncoated	-3	1
1	coated	-57.7 ± 7.8	4
2	coated	-53.9 ± 2.9	4
3	coated	-46.6 ± 9.0	6
many	coated	-40.2 ± 14.2	7
graphite	coated	0	2

[a] All bands were fitted to a single Lorentzian peak, and the number of flakes on which the measurements were made is indicated.

Since the shift of the 2D Raman band with strain, $d\omega_{2D}/d\varepsilon$, is proportional to the effective Young's modulus of the graphene, it follows that, if the polymer–graphene interface remains intact, the band shift rates in Table 1 are an indication of the efficiency of internal stress transfer within the graphene layers. Consider, first of all, the situation with the coated and uncoated monolayer and bilayers (*e.g.*, Figure 1). The value of $d\omega_{2D}/d\varepsilon$ is similar in the coated and uncoated monolayer and also similar to that of the coated bilayer. In contrast $d\omega_{2D}/d\varepsilon$ is significantly lower for the uncoated bilayer, which implies poorer stress transfer through the bilayer. In this case, the efficiency of stress transfer, k_i, can be determined from $(d\omega_{2D}/d\varepsilon)_{Uncoated}$, the measured value of the slope for the uncoated specimen, using the following equation (see Supporting Information):

$$(d\omega_{2D}/d\varepsilon)_{Uncoated} = \frac{(d\omega_{2D}/d\varepsilon)_{Monolayer}}{[n_l - k_i(n_l - 1)]} \quad (1)$$

where $(d\omega_{2D}/d\varepsilon)_{Monolayer}$ is the slope measured for a graphene monolayer and n_l is the number of layers. The value of k_i in this case calculated from the data in Table 1 using eq 1 is found to be about 0.8 (see Supporting Information).

This analysis can be extended to the case of coated many-layer flakes (see Supporting Information), where the equation is modified to give for $n_l > 2$

$$(d\omega_{2D}/d\varepsilon)_{Coated} = \frac{(d\omega_{2D}/d\varepsilon)_{Monolayer}}{[(n_l/2) - k_i((n_l/2) - 1)]} \quad (2)$$

where $(d\omega_{2D}/d\varepsilon)_{Coated}$ is the measured slope for the coated multilayer region. Using eq 2 the data in Table 1 lead to $k_i \approx 0.6$ for stress transfer between the layers in multilayer graphene (see Supporting Information). This analysis is rather simplistic, but it demonstrates clearly that internal stress transfer is less than 100% efficient for both uncoated and coated graphene flakes. Moreover, it is known that each layer of the graphene absorbs 2.3% of the light,[44] and so the Raman laser beam will penetrate only the outer layers of a multilayer flake. Hence the measured band shift for the many-layer flake comes primarily from layers near the surface, and this should be taken into account in a more thorough analysis.

The relatively weak van der Waals bonding between the individual graphene layers of graphite allows sliding between the layers to take place relatively easily, like the shearing of a deck of cards, leading to the low-friction properties of graphite. The frictional characteristics of graphene have recently been investigated using friction force microscopy, and it is found that the friction on SiC is reduced greatly by the presence of a graphene monolayer, which is reduced by a further factor of 2 for bilayer graphene.[45] In a systematic investigation upon different graphene samples with up to four layers, it was found that the friction decreased monotonically as the number of graphene layers increased[46] and tended toward the value for the bulk material value. It appears, therefore, that this easy shear between the graphene layers controls the dependence of both the frictional behavior and efficiency of stress transfer upon the number of layers in a graphene flake.

It is worthwhile to consider the implications of these findings upon the design of graphene-based nanocomposites. If we take the parameter $(d\omega_{2D}/d\varepsilon)_{Measured}$ as an indication of the ability of the graphene to reinforce a polymer matrix, then the first finding is that *bilayer graphene will be equally as good as monolayer graphene*. Moreover, only around 15% of the reinforcing efficiency is lost with trilayer graphene. In fact, if k_i is taken as 0.6, then it is only when $n_l > 7$ that the reinforcing efficiency of the graphene falls to less than half of that of the monolayer material (see Supporting Information).

As well as the number of layers in a graphene flake being important for reinforcement, it has already been established that lateral dimensions of the flake have a major effect as well.[36] Mapping of strains across a monolayer flake combined with shear-lag analysis has revealed that when a flake is deformed in a nanocomposite, the strain builds up from zero at the edges to be the same as that in the matrix in the center of the flake, if the flake is large enough (typically >10 μm).[36] Obtaining large exfoliated flakes in significant quantities remains something of a challenge.[47] Because of this, the strain was mapped in the bilayer

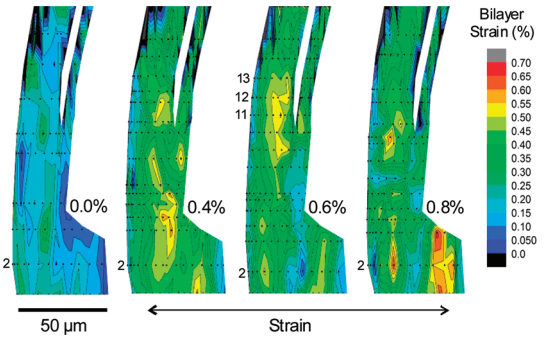

Figure 4. Maps of strain in the graphene bilayer regions of the flake shown in Figure 2, determined from the shift of the 2D1A component of the 2D Raman band, for different levels of matrix strain in the direction indicated by the arrow (laser excitation 633 nm). The black dots indicate where measurements were taken, and the individual rows of data analyzed later are marked. The monolayer and trilayer regions in the flake have been masked out for clarity.

region over the flake shown in Figure 2 at different levels of matrix strain, ε_m, using the strong 2D1A component of the bilayer 2D band, and the results are given in Figure 4.

It can be seen that there is initially ($\varepsilon_m = 0.0\%$) a small amount of residual strain in the bilayer graphene, but that when ε_m is increased to 0.4%, strain develops in the middle regions of the graphene bilayer, falling away at the edges. When the matrix strain is increased further, the distribution of strain in the graphene becomes less uniform and areas of both high and low strain develop in the middle regions of the flake.

The observation of the variation of strain across the flake at different strain levels gives further insight into the variety of deformation processes of the bilayer in the nanocomposite. Figure 5 shows the variation of strain along row 2 (see Figure 4) at different levels of matrix strain ε_m. Initially there appears to be a residual strain at the left-hand end of the flake, possibly as a result of the fabrication process and coating. At ε_m = 0.4% the strain builds up to a plateau value of around 0.4% strain, dipping down slightly in the middle of the flake. It then falls to zero at the right-hand end. The plots at ε_m = 0.6% and 0.8% strain are similar to each other, showing two triangular distributions across the flake, with the strain falling to zero at either end and also in the middle of the flake. This behavior has been seen before for a large monolayer flake[37] and was attributed to the development of cracks in the SU-8 polymer coating, although a recent study has suggested that it also could be due to cracking of the graphene.[25] Inspection of the map for ε_m = 0.8% in Figure 4 shows that similar large "peaks" and deep "valleys" have developed in the strain distribution for the graphene bilayer.

The triangular-shaped strain distributions are characteristic of frictional stress transfer at the graphene–polymer interface, and it is possible to estimate the shear stress at this interface, τ_i, from the slopes

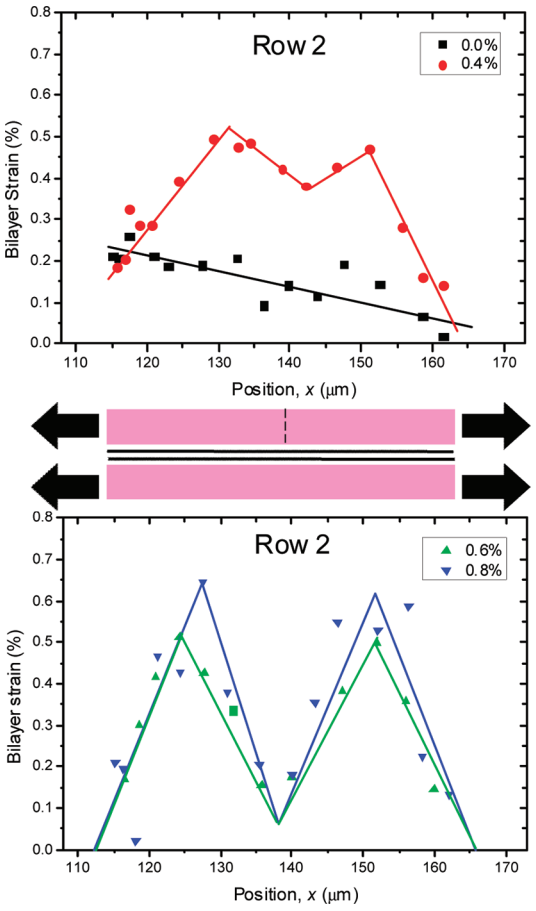

Figure 5. Variation of strain in the graphene bilayer with position along row 2 (indicated in Figure 4), at different levels of matrix strain, ε_m, showing the development of a matrix crack (see schematic diagram).

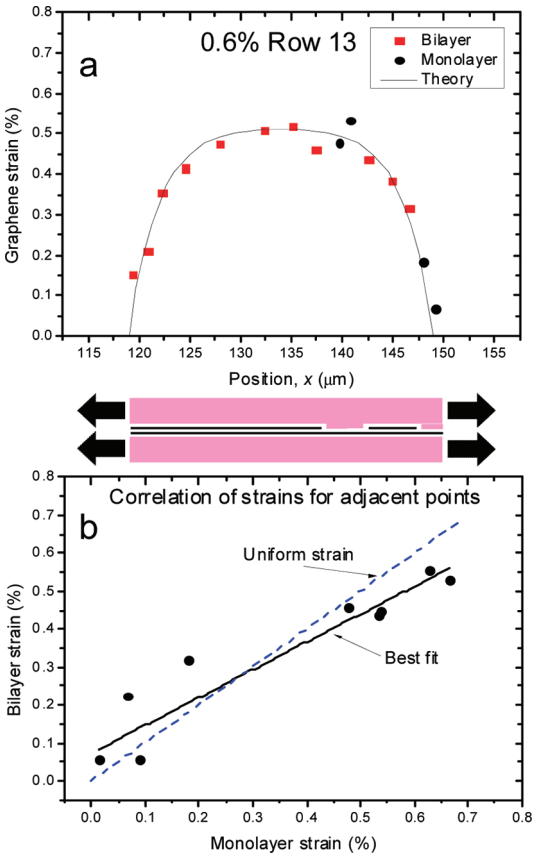

Figure 6. (a) Variation of strain in the monolayer and bilayer regions of graphene with position along row 13 (indicated in Figure 4) at an applied strain of 0.6%. The theoretical curve is a fit to the data points using eq 4 derived from shear-lag theory with $ns = 10$. (b) Correlation of measured strains in adjacent regions of the monolayer and bilayer graphene in rows 11−13 (Figure 4) at 0.6% applied strain. (The schematic diagram shows the variation of the number of graphene layers across the row.)

of the lines in Figure 5 using the force balance equilibrium[36,38]

$$\frac{d\varepsilon_f}{dx} = -\frac{\tau_i}{E_f t} \quad (3)$$

where ε_f is the strain in the flake at a position, x, E_f is the modulus of the flake (~1000 GPa), and t is its thickness (~0.7 nm for the bilayer). Putting the measured slopes from Figure 5 into this equation gives a value of interfacial shear stress that increases from 0.15 MPa at 0.4% matrix strain to around 0.3 MPa at 0.8% matrix strain.

The variation of strain across the flake in the direction of tensile straining was also determined along rows of data points along the top of the flake, where there are regions of adjacent monolayer and bilayer material (see Figure 2b). Figure 6a shows the strain variation in the bilayer and monolayer regions along row 13 at 0.6% matrix strain. The graphene strain was determined using the monolayer and bilayer calibrations from Figure 3b, and the graphene structure along the row is also shown in the schematic diagram in Figure 6. It can be seen that in this case there is a continuous variation of graphene strain along the row, indicating elastic stress transfer across the graphene−polymer interface. The data points in Figure 6a were fitted to shear-lag theory using the equation[36]

$$\varepsilon_f = \varepsilon_m \left[1 - \frac{\cosh\left(ns\frac{x}{l}\right)}{\cosh(ns/2)}\right] \quad (4)$$

where l is the length of the region being scanned across the flake and the value of ns, the fitting parameter, is 10. The points all fall close to the theoretical line, giving further support to the observation that continuum mechanics is still applicable at the nanoscale, even though the strain distributions may vary in detail between different places on the flake (*cf.* Figures 5 and 6).

The parameter s is the aspect ratio of the flake equal to l/t, where t is the flake thickness. It may be significant that in a previous study that mapped strain along a graphene monolayer flake the data could be fitted best to eq 4 using a value of $ns = 20$. This may be explained as follows: because the bilayer graphene is twice the

thickness of monolayer graphene, the aspect ratio, *s*, will be halved for a flake of bilayer material of the same length, *l*. It should also be noted, however, that the value of *n* depends upon $t^{1/2}$, and so this needs to be taken into account as well.[36]

The continuity of strain between monolayer and bilayer regions was investigated further, and similar measurements were also undertaken along rows 11 and 12 (Figure 4). Figure 6b shows the correlation between the strain measured for adjacent points in rows 11−13 at a matrix strain of 0.6%. It can be seen that the data fall close to the line for uniform strain. This confirms the finding above that there is the same level of reinforcing efficiency for both monolayer and bilayer graphene.

At this stage it is worth considering the relative advantage of using bilayer graphene compared with the monolayer material. If we take two monolayer flakes dispersed well in a polymer matrix, the closest separation they can have will be on the order of the dimension of a polymer coil, *i.e.*, at least several nanometers.[48] In contrast the separation between the two atomic layers in bilayer graphene is only around 0.34 nm, and so it will be easier to achieve higher loadings of the bilayer material in a polymer nanocomposite, leading to an improvement in reinforcement ability by up to a factor of 2 over the monolayer material.

It is possible to determine the optimum number of layers needed in the graphene flakes for the best levels of reinforcement in polymer-based nanocomposites. It was pointed out above that the effective Young's modulus of monolayer and bilayer graphene is similar and that it decreases as the number of layers decreases (see Supporting Information). In high volume fraction nanocomposites it will be necessary to accommodate the polymer coils between the graphene flakes, and the coil dimensions will limit the separation of the flakes, as shown schematically in Figure 7. Similar issues have been considered by Klein and Luckham[49] for polymer solutions between parallel mica platelets and also by de Gennes.[50] The minimum separation of the graphene flakes will depend upon the type of polymer (*i.e.*, its chemical structure and molecular conformation) and its interaction with the graphene. It is unlikely that the minimum separation will be less than 1 nm and more likely that it will be several nanometers. The separation of the layers in multilayer graphene, on the other hand, is on the order of 0.34 nm.

If a nanocomposite is assumed to be made up of parallel graphene flakes separated by a thin polymer layer of the same uniform thickness (Figure 7), then it is possible to show that for a given polymer layer thickness, the maximum volume fraction of graphene in the nanocomposite will increase with the number of layers in the graphene, as shown in Figure 8a. The Young's modulus, E_c, of such a nanocomposite can be

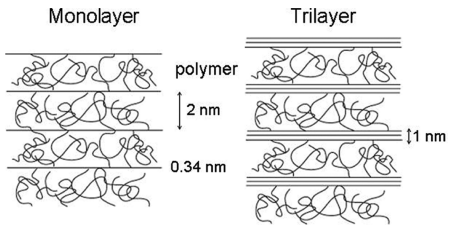

Figure 7. Schematic diagram of the microstructure of graphene-based nanocomposites based on either monolayer or trilayer reinforcements. The interlayer spacing of the graphene is 0.34 nm, and the effective thickness of the polymer coils is assumed to be around 2 nm.

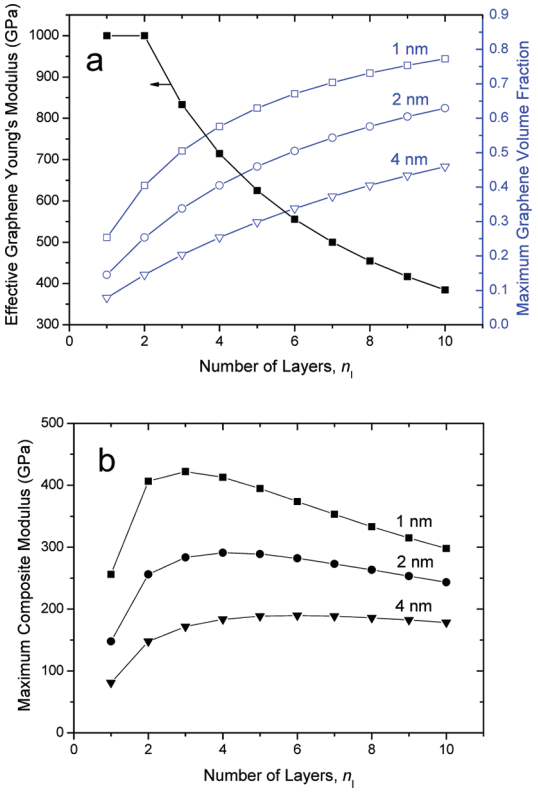

Figure 8. (a) Effective graphene Young's modulus, E_{eff}, and maximum graphene volume fraction for different indicated polymer layer thicknesses, as a function of the number of layers, n_l, in the graphene flakes. (b) Maximum nanocomposite modulus predicted for different indicated polymer layer thicknesses as a function of the number of layers, n_l, in the graphene flakes.

determined using the simple "rule-of-mixtures" model such as[48]

$$E_c = E_{eff}V_g + E_mV_m \quad (5)$$

where E_{eff} is the effective Young's modulus of the multilayer graphene, E_m is the Young's modulus of the polymer matrix (~3 GPa), and V_g and V_m are the volume fractions of the graphene and matrix, respectively ($V_g + V_m = 1$). The maximum nanocomposite Young's modulus can be determined using this equation along with the data in Figure 8a and is shown in Figure 8b as a function of n_l for polymer layers of different thickness. It can be seen that it peaks at $n_l = 3$

for a polymer layer thickness of 1 nm and then decreases, and the number of graphene layers in the flakes and polymer thickness increase. For a layer thickness of 4 nm the maximum nanocomposite Young's modulus is virtually constant for $n_l > 5$. This analysis assumes that the graphene flakes are infinitely long, but the maximum Young's modulus will be reduced for flakes of finite length because of shear-lag effects at the flake edge (Figure 6a). The exact form of plots such as Figure 8b and optimum value of n_l will depend upon the value of the stress transfer efficiency factor, k_i, but it serves as a useful design guide for graphene-based nanocomposites.

CONCLUSIONS

It has been demonstrated that although there is good stress transfer between a polymer matrix and monolayer graphene, monolayer graphene is not the optimum material to use for reinforcement in graphene-based polymer nanocomposites. There is also good stress transfer from the polymer matrix to the bilayer material and no slippage between the layers when it is fully encapsulated in a polymer matrix. Less efficient stress transfer has been found for trilayer and many-layer graphene due to slippage between the internal graphene layers, indicating that such materials will have a lower effective Young's modulus than either monolayer or bilayer graphene in polymer-based nanocomposites. However, since the interlayer spacing in multilayer graphene is only 0.34 nm and so an order of magnitude less than the dimensions of polymer coils, higher volume fractions of graphene can be obtained for multilayer material. There is therefore a balance to be struck in the design of graphene-based nanocomposites between the ability to achieve higher loadings of reinforcement and the reduction in effective Young's modulus of the reinforcement as the number of layers in the graphene is increased.

MATERIALS AND METHODS

The specimens were prepared using 5 mm thick poly(methyl methacrylate) beams spin-coated with 300 nm of cured SU-8 epoxy resin as described elsewhere.[36,37] The graphene was produced by mechanical cleaving of graphite and deposited on the surface of the SU-8. For some beams a thin, 300 nm layer of SU-8 was then spin-coated on top and cured so that the graphene remained visible when sandwiched between the two coated polymer layers. This method produced graphene with a range of different numbers of layers that were identified both optically and by using Raman spectroscopy.[10,11] The PMMA beams were deformed in 4-point bending up to 0.4% strain with the strain monitored using a strain gage attached to the beam surface. Well-defined Raman spectra could be obtained from the graphene with different numbers of layers, using either a low-power (<1 mW at the sample) HeNe laser (1.96 eV) or near IR laser (1.58 eV) in Renishaw 1000 or 2000 spectrometers. The laser beam polarizations were always parallel to the tensile axis, and the spot size of the laser beams on the sample was approximately 2 μm using a 50$\times$ objective lens.

One uncoated beam was unloaded after initial measurements had been made and then coated with a layer of cured SU-8. The beam was reloaded initially up to 0.4% strain, and the deformation of the monolayer and bilayer graphene on the same flake on the surface of the beam was again followed from the shift of the 2D (or G′) Raman band. The beam was then unloaded and then reloaded to various other levels of strain, and the shift of a trilayer region on the same flake and a many-layer graphene flake was also followed from the shift of the 2D (or G′) Raman band.

The strains in the graphene flake containing both monolayer and bilayer regions were mapped fully at each strain level as well as in the unloaded state. Raman spectra were obtained at different strain levels through mapping over the graphene monolayer in steps of between 2 and 5 μm by moving the $x-y$ stage of the microscope manually and checking the position of the laser spot on the specimen relative to the image of the monolayer on the screen of the microscope. The strain at each measurement point was determined from the position of the 2D Raman band using the calibrations in Figure 1, and strain maps of the bilayer were produced in the form of colored $x-y$ contour maps using the OriginPro 8.5 graph-plotting software package, which interpolates the strain between the measurement points. One-dimensional plots of the variation of strain across the flake were also plotted along the rows indicated in Figure 4, at different levels of matrix strain.

Conflict of Interest: The authors declare no competing financial interest.

Acknowledgment. The authors of this work are grateful to the Engineering and Physical Sciences Research Council for support in the form of a Science and Innovation Award (EP/G035954/1). One of the authors (A.S.N.) is also supported by the Royal Society.

Supporting Information Available: (S1) Deformation of the bilayer graphene, (S2) deformation of different graphene flakes, (S3) adaption of the theory of Zalamea, Kim, and Pipes to multilayer graphene. This material is available free of charge *via* the Internet at http://pubs.acs.org.

REFERENCES AND NOTES

1. Geim, A. K.; Novoselov, K. S. The Rise of Graphene. *Nat. Mater.* **2007**, *6*, 183–190.
2. Novoselov, K. S. Nobel Lecture: Graphene: Materials in the Flatland. *Rev. Mod. Phys.* **2011**, *83*, 837–849.
3. Geim, A. K. Nobel Lecture: Random Walk to Graphene. *Rev. Mod. Phys.* **2011**, *83*, 851–862.
4. Novoselov, K. S.; Geim, A. K.; Morozov, S. V.; Jiang, D.; Zhang, Y.; Dubonos, S. V.; Grigorieva, I. V.; Firsov, A. A. Electric Field Effect in Atomically Thin Carbon Films. *Science* **2004**, *306*, 666–669.
5. Novoselov, K. S.; Geim, A. K.; Morozov, S. V.; Jiang, D.; Katsnelson, M. I.; Grigorieva, I. V.; Dubonos, S. V.; Firsov, A. A. Two-dDimensional Gas of Massless Dirac Fermions in Graphene. *Nature* **2005**, *438*, 197–200.
6. Y Zhang, Y. B.; Tan, Y. W.; Stormer, H. L.; Kim, P. Experimental Observation of the Quantum Hall Effect and Berry's Phase in Graphene. *Nature* **2005**, *438*, 201–204.
7. Zhang, F.; Min, H.; Polini, M.; MacDonald, A. H. Spontaneous Inversion Symmetry Breaking in Graphene Bilayers. *Phys. Rev. B* **2010**, *81*, 041402.
8. Mayorov, A. S.; Elias, D. C.; Mucha-Kruczynski, M.; Gorbachev, R. V.; Tudorovskiy, T.; Zhukov, A.; Morozov, S. V.; Katsnelson, M. I.; Fal'ko, V. I.; Geim, A. K.; Novoselov, K. S. Interaction-Driven Spectrum Reconstruction in Bilayer Graphene. *Science* **2011**, *333*, 860–863.
9. Lee, C.; Wei, X. D.; Kysar, J. W.; Hone, J. Measurement of the Elastic Properties and Intrinsic Strength of Monolayer Graphene. *Science* **2008**, *321*, 385–388.

10. Ferrari, A. C.; Meyer, J. C.; Scardaci, V.; Casiraghi, C.; Lazzeri, M.; Mauri, F.; Piscanec, S.; Jiang, D.; Novoselov, K. S.; Roth, S.; Geim, A. K. Raman Spectrum of Graphene and Graphene Layers. *Phys. Rev. Lett.* **2006**, *97*, 187401.
11. Malard, L. M.; Pimenta, M. A.; Dresselhaus, G.; Dresselhaus, M. S. Raman Spectroscopy in Graphene. *Phys. Rep.* **2009**, *473*, 51–87.
12. Ni, Z. H.; Yu, T.; Lu, Y. H.; Wang, Y. Y.; Feng, Y. P.; Shen, Z. X. Uniaxial Strain on Graphene: Raman Spectroscopy Study and Band-Gap Opening. *ACS Nano* **2008**, *2*, 2301–2305.
13. Yu, T.; Ni, Z. H.; Du, C. L.; You, Y. M.; Wang, Y. Y.; Shen, Z. X. Raman Mapping Investigation of Graphene on Transparent Flexible Substrate: The Strain Effect. *J. Phys. Chem. C* **2008**, *112*, 12602–12605.
14. Huang, M. Y.; Yan, H.; Chen, C. Y.; Song, D. H.; Heinz, T. F.; Hone, J. Phonon Softening and Crystallographic Orientation of Strained Graphene Studied by Raman Spectroscopy. *Proc. Natl. Acad. Sci.* **2009**, *106*, 7304–7308.
15. Mohiuddin, T. M. G.; Lombardo, A.; Nair, R. R.; Bonetti, A.; Savini, G.; Jalil, R.; Bonini, N.; Basko, D. M.; Galiotis, C.; Marzari, N.; *et al*. Uniaxial Strain in Graphene by Raman spectroscopy: G Peak Splitting, Gruneisen Parameters, and Sample Orientation. *Phys. Rev. B* **2009**, *79*, 205433.
16. Tsoukleri, G.; Parthenios, J.; Papagelis, K.; Jalil, R.; Ferrari, A. C.; Geim, A. K.; Novoselov, K. S.; Galiotis, C. Subjecting a Graphene Monolayer to Tension and Compression. *Small* **2009**, *5*, 2397–2402.
17. Proctor, J. E.; Gregoryanz, E.; Novoselov, K. S.; Lotya, M.; Coleman, J. N.; Halsall, M. P. High-Pressure Raman Spectroscopy of Graphene. *Phys. Rev. B* **2009**, *80*, 073408.
18. Metzger, C.; Remi, S.; Liu, M.; Kusminskiy, S. V.; Castro Neto, A. H.; Swan, A. K.; Goldberg, B. B. Biaxial Strain in Graphene Adhered to Shallow Depressions. *Nano Lett.* **2009**, *10*, 6–10.
19. Ferralis, N Probing Mechanical Properties of Graphene with Raman Spectroscopy. *J. Mater. Sci.* **2010**, *45*, 5135–5149.
20. Huang, M. Y.; Yan, H.; Heinz, T. F.; Hone, J. Probing Strain-Induced Electronic Structure Change in Graphene by Raman Spectroscopy. *Nano Lett.* **2010**, *10*, 4074–4079.
21. Mohr, M.; Maultzsch, J.; Thomsen, C. Splitting of the Raman 2D Band of Graphene Subjected to Strain. *Phys. Rev. B* **2010**, *82*, 201409.
22. Frank, O.; Mohr, M.; Maultzsch, J.; Thomsen, C.; Riaz, I.; Jalil, R.; Novoselov, K. S.; Tsoukleri, G.; Parthenios, J.; Papagelis, K.; *et al*. Raman 2D-Band Splitting in Graphene: Theory and Experiment. *ACS Nano* **2011**, *5*, 2231–2239.
23. Cheng, Y. C.; Zhu, Z. Y.; Huang, G. S.; Schwingenschlögl, U. Gruneisen Parameter of the G Mode of Strained Monolayer Graphene. *Phys. Rev. B* **2011**, *83*, 115449.
24. Frank, O.; Tsoukleri, G.; Riaz, I.; Papagelis, K.; Parthenios, J.; Ferrari, A. C.; Geim, A. K.; Novoselov, K. S.; Galiotis, C. Development of a Universal Stress Sensor for Graphene and Carbon Fibres. *Nat. Commun.* **2011**, *2*, 255.
25. Frank, O.; Bouša, M.; Riaz, I.; Jalil, R.; Novoselov, K. S.; Tsoukleri, G.; Parthenios, J.; Kavan, L.; Papagelis, K.; Galiotis, C. Phonon and Structural Changes in Deformed Bernal Stacked Bilayer Graphene. *Nano Lett.* **2012**, dx.doi.org/10.1021/nl203565p.
26. Galiotis, C; Robinson, I. M.; Young, R. J.; Smith, B. J. E.; Batchelder, D. N. Strain Dependence of the Raman Frequencies of a Kevlar 49 Fibre. *Polym. Commun.* **1985**, *26*, 354–355.
27. Day, R. J.; Robinson, I. M.; Zakikhani, M.; Young, R. J. Raman-Spectroscopy of Stressed High Modulus Poly(p-phenylene benzobisthiazole) Fibers. *Polymer* **1987**, *28*, 1833–1840.
28. Robinson, I. M.; Zakikhani, M.; Day, R. J.; Young, R. J.; Galiotis, C. Strain Dependence of the Raman Frequencies for Different Types of Carbon-Fibres. *J. Mater. Sci. Lett.* **1987**, *6*, 1212–1214.
29. Huang, Y.; Young, R. J. Effect of Fiber Microstructure upon the Modulus of PAN- and Pitch-Based Carbon Fibers. *Carbon* **1995**, *33*, 97–107.
30. Huang, Y. L.; Young, R. J. Analysis of the Fragmentation Test for Carbon-Fiber Epoxy Model Composites by Means of Raman Spectroscopy. *Compos. Sci. Technol.* **1994**, *52*, 505–517.
31. Huang, Y; Young, R. J. Interfacial Behavior in a High-Temperature Cured Carbon Fibre/Epoxy Resin Model Composite. *Composites, Part A* **1995**, *26*, 541–550.
32. Montes-Moran, M. A.; Young, R. J. Raman Spectroscopy Study of HM Carbon Fibres: Effect of Plasma Treatment on the Interfacial Properties of Single Fibre/Epoxy Composites—Part I: Fibre Characterization. *Carbon* **2002**, *40*, 845–855.
33. van den Heuvel, P. W. J.; Peijs, T.; Young, R. J. Failure Phenomena in Two-Dimensional Multi-Fibre Microcomposites 2. A Raman Spectroscopic Study of the Influence of Inter-Fibre Spacing on Stress Concentrations. *Compos. Sci. Technol.* **1997**, *57*, 899–911.
34. Cooper, C. A.; Young, R. J.; Halsall, M. Investigation into the Deformation of Carbon Nanotubes and their Composites through the Use of Raman Spectroscopy. *Composites, Part A* **2001**, *32*, 401–411.
35. Deng, L. B.; Eichhorn, S. J.; Kao, C. C.; Young, R. J. The Effective Young's Modulus of Carbon Nanotubes in Composites. *ACS Appl. Mater. Interfaces* **2011**, *3*, 433–440.
36. Gong, L.; Kinloch, I. A.; Young, R. J.; Riaz, I.; Jalil, R.; Novoselov, K. S. Interfacial Stress Transfer in a Graphene Monolayer Nanocomposite. *Adv. Mater.* **2010**, *22*, 2694–2697.
37. Young, R. J.; Gong, L.; Kinloch, I. A.; Riaz, I.; Jalil, R.; Novoselov, K. S. Strain Mapping in a Graphene Monolayer Nanocomposite. *ACS Nano* **2011**, *5*, 3079–3084.
38. Kelly, A.; Macmillan, N. H. *Strong Solids*, 3rd ed.; Clarendon Press: Oxford, 1986.
39. Srivastava, I.; Mehta, R. J.; Yu, Z.-Z.; Schadler, J.; Koratkar, N. Raman Study of Interfacial Load Transfer in Graphene Nanocomposites. *Appl. Phys. Lett.* **2011**, *98*, 063102.
40. Gao, Y.; Liu, L.-Q.; Zu, S.-Z.; Peng, K.; Zhou, D.; Han, B.-H.; Zhang, Z. The Effect of Interlayer Adhesion on the Mechanical Behaviors of Macroscopic Graphene Oxide Papers. *ACS Nano* **2011**, *5*, 2134–2141.
41. Zalamea, L.; Kim, H.; Pipes, R. B. Stress Transfer in Multi-Walled Carbon Nanotubes. *Compos. Sci. Technol.* **2007**, *67*, 3425–3433.
42. Cui, S.; Kinloch, I. A.; Young, R. J.; Noe, L.; Monthioux, M. The Effect of Stress Transfer Within Double-Walled Carbon Nanotubes Upon Their Ability to Reinforce Composites. *Adv. Mater.* **2009**, *21*, 3591–3596.
43. Ding, F.; Xu, Z. W.; Yakobson, B. I.; Young, R. J.; Kinloch, I. A.; Cui, S.; Deng, L. B.; Puech, P; Monthioux, M. Formation Mechanism of Peapod-Derived Double-Walled Carbon Nanotubes. *Phys. Rev. B* **2010**, *82*, 041403.
44. Nair, R. R.; Blake, P.; Grigorenko, A. N.; Novoselov, K. S.; Booth, T. J.; Stauber, T.; Peres, N. M. R.; Geim, A. K. Fine Structure Constant Defines Visual Transparency of Graphene. *Science* **2008**, *320*, 1308–1308.
45. Filleter, T.; McChesney, J. L.; Bostwick, A.; Rotenberg, E.; Emtsev, K. V.; Seyller, Th.; Horn, K.; Bennewitz, R. Friction and Dissipation in Epitaxial Graphene Films. *Phys. Rev. Lett.* **2009**, *102*, 086102.
46. Lee, C.; Li, Q. Y.; Kalb, W.; Liu, X.-Z.; Berger, H.; Carpick, R. W.; Hone, J. Frictional Characteristics of Atomically Thin Sheets. *Science* **2010**, *328*, 76–80.
47. Hernandez, Y.; Nicolosi, V.; Lotya, M.; Blighe, F. M.; Sun, Z. Y.; De, S.; McGovern, I. T.; Holland, B.; Byrne, M.; Gun'ko, Y. K.; *et al*. High-Yield Production of Graphene by Liquid-Phase Exfoliation of Graphite. *Nat. Nanotechnol.* **2008**, *3*, 563–568.
48. Young, R. J.; Lovell, P. A. *Introduction to Polymers*, 3rd ed.; CRC Press: Boca Raton, 2011.
49. Klein, J.; Luckham, P. F. Long-Range Attractive Forces between Two Mica Surfaces in an Aqueous Solution. *Nature* **1984**, *308*, 836–837.
50. de Gennes, P. G. Polymers at an Interface: A Simplified View. *Adv. Polym. Sci.* **1987**, *27*, 189–209.